The structure and electronic characteristics of metallosilicates with ZSM-5 structure

Yasunori Oumi, Michiyuki Yamadaya, Tomonori Kanougi, Momoji Kubo, András Stirling *, Rajappan Vetrivel ‡, Ewa Broclawik § and Akira Miyamoto

Department of Molecular Chemistry and Engineering, Faculty of Engineering, Tohoku University, Sendai 980-77, Japan

Received 30 May 1996; accepted 19 February 1997

We report here the result of a computer-assisted study of metallosilicates by applying molecular dynamics (MD) and quantum chemical (QC) methods. MD calculations are used to study the local relaxation in the T12 site of the ZSM-5 structure, when Si is substituted by different metals such as Ti^{4+}, Al^{3+}, Ga^{3+}, and Fe^{3+}. QC calculations by density functional theory have been performed on the cluster models generated from the structure obtained by MD calculations. The calculation indicates that the net charge on a MO_4 (where M = Ti, Al, Ga, and Fe) group and the molecular electrostatic potential values are good parameters to assess the acidic properties of metallosilicates, as shown by their correlations to the reported experimental acidity.

Keywords: ZSM-5 structure, metallosilicates, molecular dynamics (MD), density functional theory (DFT) calculations, molecular electrostatic potential (MEP)

1. Introduction

Since the commercial utilization of zeolite-Y for catalytic cracking in 1963 [1], the search for newer zeolites with novel catalytic properties has been continuing. Zeolites with unusual pore architectures are reported in the literature [2,3]. Another direction of research, to tune the properties of zeolites on a finer scale, is to replace the Si^{4+} by Al^{3+} and many other metals [4,5]. The catalytic properties certainly have a crucial dependence on the nature and amount of the metals. Usually, metals are present inside the pores of zeolites as exchanged cations, framework cations in place of Si^{4+} in the lattice in the form of metal oxides in the pores.

It is indeed difficult to obtain information about the particular state of the metal inside the zeolites. Different analytical techniques and their combinations could not provide unambiguous results. It is more often true that the metal concentration is too low (Si^{4+}/M ratio is too high) to allow structural characterization. XRD could neither locate the framework position nor provide the local geometry around the metal cation. EXAFS studies have recently been applied to derive the local geometry and have led to contradicting reports [6,7]. We have applied computational techniques such as classical and quantum chemical methods to study metallosilicates (where metals replace Si^{4+} in the framework). In this paper, we report the results of our study, where we have combined the power of both molecular dynamics (MD) calculations and quantum chemical–density functional theory (QC-DFT) calculations.

2. Methodology

The MD calculations were carried out with the MXDORTO program developed by Kawamura [8]. The Verlet algorithm [9] was used for calculation of the atomic motions, while the Ewald method [10] was applied for the calculation of the electrostatic interactions. Temperature and pressure were controlled by means of scaling the atom velocities and unit cell parameters under three-dimensional periodic boundary conditions. The two-body central force interatomic potential, eq. (1), was used for all calculations:

$$U_{ij}(r_{ij}) = \frac{Z_i Z_j e^2}{r_{ij}} + f_0(b_i + b_j)\exp\left(\frac{a_i + a_j - r_{ij}}{b_i + b_j}\right), \quad (1)$$

where Z_i is the atomic charge, e is the elementary electronic charge, r_{ij} is the interatomic distance, and f_0 is a constant. In this equation, the first and second terms refer to Coulomb and repulsive interactions, respectively [11–13]. The parameters a_i and b_i represent the size and stiffness of the atoms, respectively, in the repulsive interactions. Table 1 shows the potential parameters employed in this study. The details and effectiveness of the two-body interatomic potential for reproducing the experimentally determined crystal structure of ZSM-5 as well as other conditions of the simulations have been reported elsewhere [13].

* On leave from: Institute of Isotopes, Hungarian Academy of Sciences, PO Box 77, H-1525 Budapest, Hungary.
‡ Present address: Catalysis Division, National Chemical Laboratory, Pune 411008, India.
§ Present address: Institute of Catalysis, Polish Academy of Sciences, PL-30239 Krakow, Poland.

Table 1
Potential parameters used for MD calculations

Atom	Z_i	a_i (Å^{-1})	b_i (Å^{-1})
O	−2.0	1.629	0.085
Si	4.0	1.012	0.080
Ti	4.0	1.235	0.080
Al	3.0	1.076	0.080
Ga	3.0	1.076	0.080
Fe	3.0	0.801	0.080

DFT (density functional theory) quantum chemical calculations [14,15] were performed using the DMol package of BIOSYM, Inc., USA [16]. The geometry optimization calculations were carried out using a minimal numerical basis set [17]. A Janak–Moruzzi–Williams (JMW) type local correlation functional [18] was used for the exchange–correlation energy terms in the total energy expression. The total energy of the final optimized geometry was evaluated using a double numerical polarization basis set with nonlocal gradient corrected potential for exchange [19] and correlation terms [20].

Calculations were performed on Hewlett-Packard HP9000 model 712/60 and Silicon Graphics INDY R4400 workstations, while the static visualization was done with the Insight II program developed by BIOSYM, Inc., USA. The dynamic visualization was made with the MOMOVIE and RYUGA codes [21] developed in our laboratory on OMRON LUNA-88K and Hewlett-Packard HP9000 model 712/60 workstations, respectively.

3. Model

The physical and chemical state of the substituted metal in a H-metallosilicate has not been unequivocally established so far. However, there is some evidence that the metal is present in highly dispersed monomeric form, coordinated to basic oxygens within the zeolite channels. The ultimate state of the metal may vary depending upon the conditions under which the catalyst works. There are twelve different T sites in the ZSM-5 structure where Si^{4+} can be substituted with another metal. For aluminosilicate, there are several reports using quantum chemical methods which demonstrated that the T12 site is the energetically favorable site when a silicon in the zeolite is substituted by an aluminum atom [22,23]. Although the substituted site may be different depending on the nature of the substituted metal, we considered the T12 site as a typical single site for metal substitution in all calculations for comparison of the influence of metal substitution.

The crystal structure of ZSM-5 determined by X-ray diffraction [24] was taken as the initial structure for all MD simulations. The geometry of the cluster model for quantum chemical calculations has been derived from the structure obtained from MD simulation. The stoichiometry of the cluster model is H_6TSiO_7 (T = Ti^{4+}, Al^{3+}, Ga^{3+}, or Fe^{3+}) to represent the zeolitic framework. Adjacent silicon atoms bonded to oxygen atoms were replaced by hydrogen atoms, which is obviously not perfect but a frequently used methodology of saturating dangling bonds on cluster boundaries. Selecting the proper cluster for zeolitic structures is itself a subject of many studies [25–27]. Our choice is rather a modest one, bearing in mind that the local structure around the incorporated metal center is our interest. We believe that this cluster is adequate for reproducing basic features of a local electronic structure of an active center in the zeolitic framework. On the other hand, it offers the possibility of employing the highest level of computational accuracy required for the evaluation of electronic properties.

4. Results and discussion

4.1. MD calculations

Earlier, we have carried out extensive MD calculations on a ZSM-5 structure with fully siliceous composition [28]. The overall lattice structure reported by XRD studies is well reproduced by the MD simulation. The mean square derivations of atomic positions during simulation from experimental geometry are also reported [28]. As there are several metals which can replace Si^{4+}, we have considered the substitution of M (where M = Ti^{4+}, Al^{3+}, Ga^{3+} and Fe^{3+}), for which the ionic radii are greater than that of the Si^{4+}, in the place of the Si^{4+} in the framework at the T12 site. MD calculations predict relaxations in the framework due to these substitutions [28]. When Si^{4+} is replaced by Ti^{4+}, the framework neutrality is maintained. However, when Si^{4+} is replaced by other trivalent cations, the framework becomes anionic. The anionic framework is neutralized by a proton attached to the oxygen bridging Si^{4+} and trivalent metal cations. The actual position of the proton is predicted by MD simulation and it is further refined by quantum chemical geometry optimization calculations. The Computer Graphics (CG) picture of Al-ZSM-5, where Si^{4+} is replaced by Al^{3+} at the T12 site, is shown as a typical case in figure 1. This figure demonstrates the validity of MD simulation parameters in reproducing the crystal structure of metallosilicates. Similar calculations were carried out to study the incorporation of other metals into the ZSM-5 structure, at the T12 site. The local structure variations were calculated. The MD calculations predict different local geometry around the substitution site for different metals. The dimer cluster models derived from the MD equilibrated structure for Al-ZSM-5 are shown by highlighting them as a ball and stick model in relation to the lattice in figure 2.

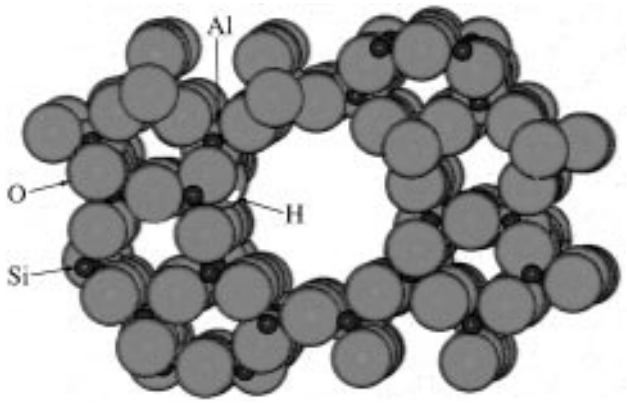

Figure 1. The CG picture of the Al-ZSM-5 lattice at 300 K after 30 000 time steps of each 1×10^{-15} s in the MD simulation. One of the T12 sites is substituted by an Al atom in the unit cell.

4.2. Local geometry obtained by MD calculations

The T12 site is bonded to four oxygen atoms, namely O11, O12, O20 and O24. These four oxygen atoms are shared by four more T sites, which are T11, T8, T3 and T12, respectively. The numbering scheme for T and O sites is as given in the crystal structure report [24]. Hence, four dimer cluster models are possible with the four different oxygen atoms as the bridging atoms. We have chosen the dimer which has the symmetrical T12–O24—T12 linkage as the typical cluster model to study the acidic properties. The bridging oxygen O24, which connects the two T12 sites is topographically at the intersection of the straight and sinusoidal channel of the ZSM-5 framework (figure 2). When a proton is attached to this oxygen as a charge compensating cation, the reactant molecules can approach this proton site from both straight and sinusoidal channels. The local geometry (M–O bond length and M–O–Si angle) around the substituted metal in relation to the all-silicon structure is given in figure 3. The order of the average M–O bond lengths, predicted by the MD simulation corresponds with that of the ionic radii of M [29]. The variation in the average M–O–Si angles is inversely proportional to the variation in the average M–O bond lengths, with the exception of Ti. The O–M–O angles did not show much variation from the equilibrium tetrahedral (109.47°) value. Thus, the MD simulation applied to derive the local geometry of metallosilicates for performing further quantum chemical cluster calculations.

4.3. Electronic structure of active sites in metallosilicate

The energetics is an indication of the stability of the bonds in the cluster models and hence the overall stability of the lattice. However, due to the small cluster models chosen in the present investigation, we reserve the energy vs. stability discussions for a future report, where a larger pentameric cluster will be used. The net charges calculated by Mulliken population analysis for the metal cation (M) and the oxygen atoms surrounding the M are given in table 2. These metallosilicates have been synthesized and their acidic properties have been reported by Innui and Matsuba [30]. They reported the maximum temperature (T_{max}) value where all the NH_3 molecules desorb from the strongest acid sites. They found that the order of acid strength of metallosilicates is $Al \geqslant Ga > Fe$. These acidic sites are mainly responsible for the acid-catalyzed reaction in hydrocarbon conver-

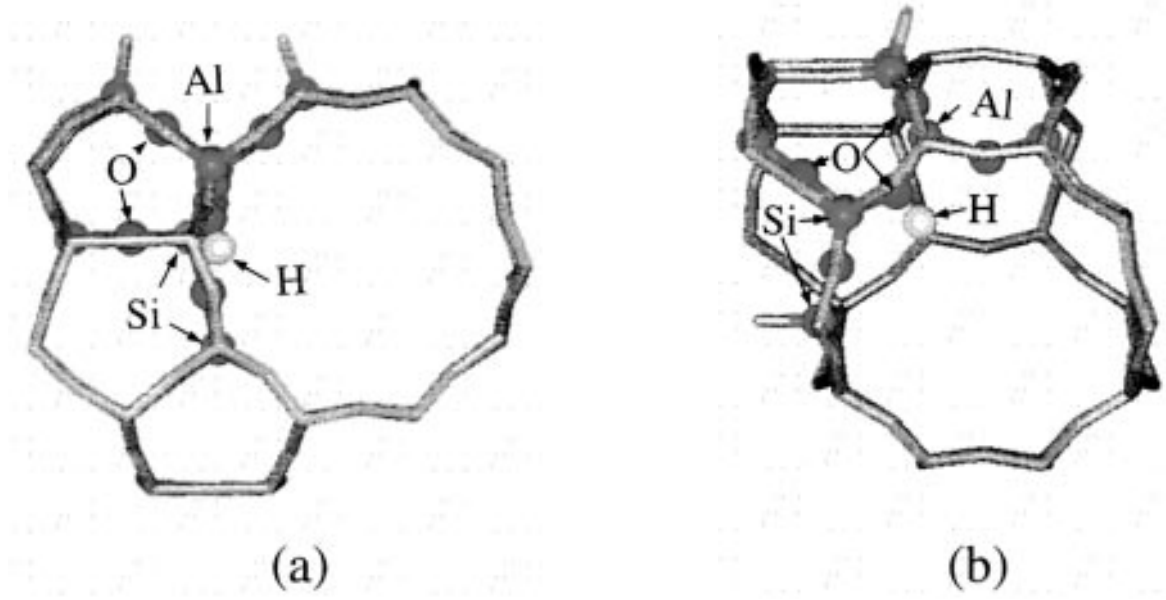

Figure 2. The CG picture of the H-$AlSiO_7H_6$ cluster at the T12 site is highlighted as ball and stick model in the MFI lattice as viewed along the straight channel in *b*-axis (a) and the sinusoidal channel in *a*-axis (b).

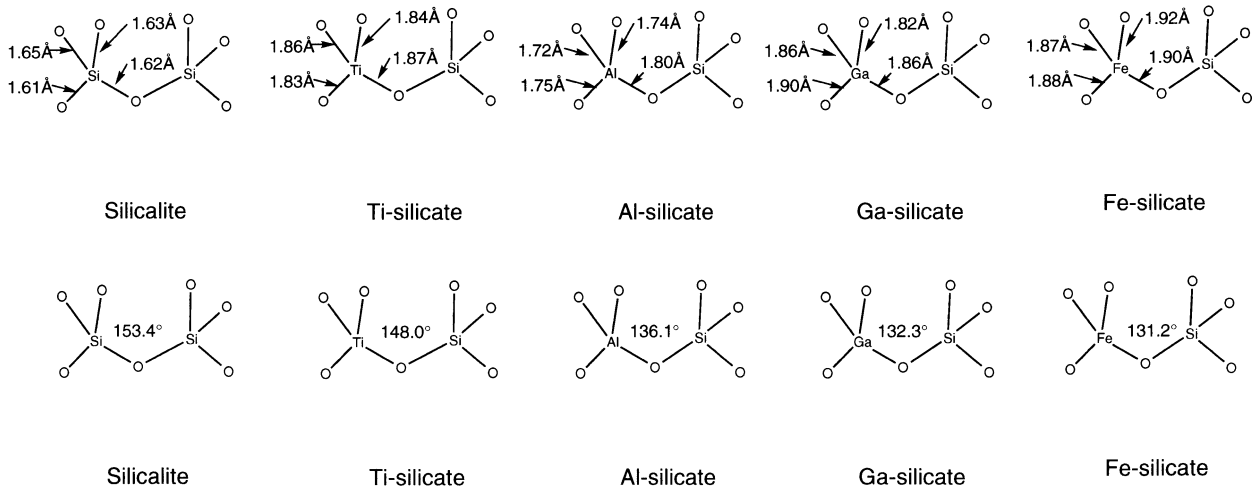

Figure 3. The local geometry of metallosilicates. T–O bond lengths and T–O–T bond angles obtained from MD simulation are shown.

sion reactions such as alkylation, isomerization, cracking etc. The net charge value on the M does not show a correlation with the experimentally reported acidity. The total net charge on the MO_4 group, however, shows a direct linear relation with the acidity. This linear relation indicates that the proton is not localized to one bridging oxygen but around the whole MO_4 group. Thus our results indicate that the electron density on the MO_4 group is a parameter which is useful to predict the acidity of metallosilicates. The charge on the proton at the bridging site also has a linear correlation with acidity. However, according to the net charge on the "MO_4" group, the acidity order is $Al \geqslant Ga > Fe$, while the net charge on the proton predicts the acidity order: $Al > Ga \sim Fe$. Although, there is quantitative correlation with the experimental observation, the reason for quantitative charges are being probed by calculations on larger cluster models. These values are obviously not available for the clusters, where Si^{4+} or Ti^{4+}.

4.4. The molecular electrostatic potential of metallosilicates

The molecular electrostatic potential (MEP) generated by the zeolite framework cluster was calculated from the electron density. The MEP maps indicate the positive and negative potentials occurring in the space around the clusters. A cubic space containing the cluster and which extends to 3 Å from its outermost atoms in all directions is considered. This cubic space is divided into 26 equally spaced regions in all three directions. The molecular electrostatic potential, $V(\boldsymbol{R})$, derived from the interaction of the molecular electronic and nuclear charge distribution with a probe charge. The probe is a hypothetical volumeless species with unit positive charge. MEP values at all the points were calculated on a grid of $26 \times 26 \times 26$ points by the method proposed by Srocoo and Tomasi [31,32] by applying the equation

$$V(\boldsymbol{R}) = -\int \frac{\rho(\boldsymbol{r})}{|\boldsymbol{R}-\boldsymbol{r}|}\,\mathrm{d}r + \sum_{\alpha=1}^{N} \frac{Z_\alpha}{|\boldsymbol{R}-\boldsymbol{R}_\alpha|}\,, \qquad (2)$$

where $\boldsymbol{R}$, $\boldsymbol{r}$ and $\boldsymbol{R}_\alpha$ are the coordinates of the probe, the electron density and the nuclei, respectively. Z_α is the nuclear charge and $\rho(\boldsymbol{r})$ is the molecular electronic charge density. Thus, the MEP is calculated at 17576 points. The positive MEP values correspond to electrophilic sites; these are shown as red contours in figure 4. The negative MEP values correspond to nucleophilic sites; these are shown as green contours. However, the interpretation of the former values requires great care because, as the probe charge approaches a nucleus, this value can be infinitely large. The 3D contour of the MEP map for the dimer cluster, $AlSiO_6H_7$ is shown in figure 4,

Table 2
Net charges of cluster models representing metallosilicates

	$Si_2O_7H_6$	$TiSiO_7H_6$	H-$FeSiO_7H_6$	H-$GaSiO_7H_6$	H-$AlSiO_7H_6$
net charge on central cation	1.06	1.55	1.13	1.29	1.03
net charge on O_{12}	−0.73	−0.86	−0.86	−0.95	−0.88
net charge on O_8	−0.70	−0.83	−0.78	−0.93	−0.83
net charge on O_3	−0.58	−0.73	−0.86	−0.89	−0.85
net charge on O_{11}	−0.71	−0.84	−0.79	−0.93	−0.84
total net charge on MO_4 tetrahedral	−1.7	−1.7	−2.2	−2.4	−2.4
net charge on compensating proton	–	–	0.58	0.59	0.63

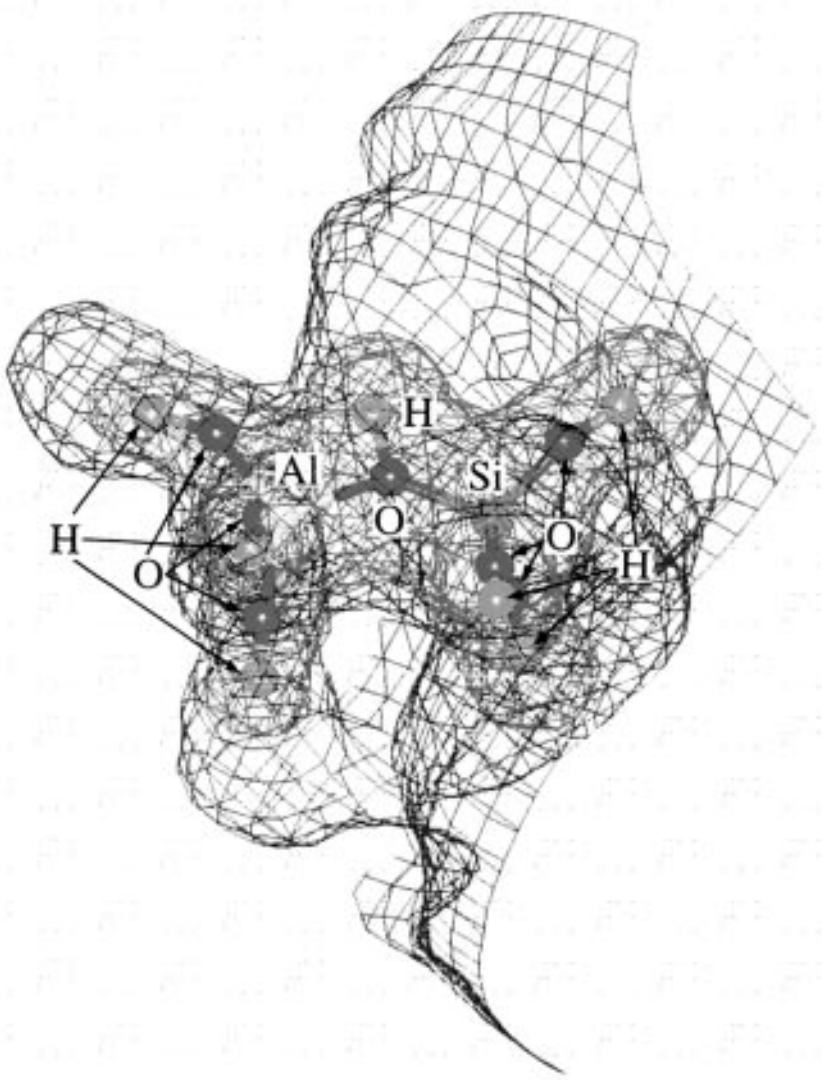

Figure 4. The 3D contour of MEP of the cluster H-$AlSiO_7H_6$; the positive and negative potential contours are shown as red and green, respectively.

as a typical example. The 3D MEP map was qualitatively the same for all the cluster models given in table 2.

We have analyzed both the positive and negative values as well as the number of occurrence of the positive and negative MEP points around the T12 site with different metal cations. The number of the grid points where the MEP has a negative value is larger for the tetravalent metal-substituted cluster than the number of the grid points where the MEP has positive values. In contrast, we observed an opposite trend for trivalent metal-substituted clusters, as shown in figure 5. These results show that the valence of the metal ion is a dominating factor in deciding the electrophilic and nucleophilic regions. Indeed, it is the trivalent metal which gives rise to the change in the MEP. In addition, we analyzed the actual values of the minima at critical points in the MEP. The critical points are the points where the MEP values have the most negative values; these values are plotted as a function of M for different cluster models in figure 6. The absolute values of MEP minima in a series of related molecules very often correlate with the protonation energy [33]. It is apparent from figure 6 that the metal substitution lowers the minimum value in each case. This effect is substantially larger for the trivalent metal than for Ti^{4+} and the Al^{3+} results in the deepest negative potential values. We can conclude that the charge/size ratio is the controlling factor in deciding the most negative MEP values. The minima points of the MEPs for the Al^{3+}-, Ga^{3+}- and Fe^{3+}-substituted clusters show that they have more negative values than the Si^{4+}- and Ti^{4+}-substituted clusters which indicates higher polarizing ability of trivalent metals and, consequently, higher acidity. Among the substitutes, Al^{3+} causes the maximum polarization followed by Ga^{3+}, and then Fe^{3+}. This trend is in good accordance with the Mulliken population values as well as the experimental acidity order [30]. These regions also can be considered

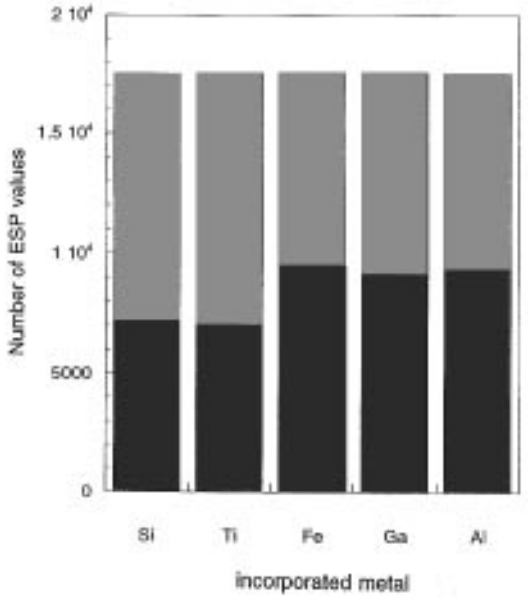

Figure 5. The bar chart showing the distribution of negative and positive electrostatic potential points in various dimer clusters with metal atom substitution. The numbers of positive and negative points are shown by dark and light shades, respectively.

as active nucleophilic regions. For example, in the case of $M = Al^{3+}$, the most negative MEP is around the oxygen atoms which are on the opposite site of H^+ bound to Al^{3+}.

5. Conclusions

MD and QC calculations have been performed to understand the structure and electronic properties of metallosilicates. For the first time, the local structure of metal-substituted zeolite framework is derived from MD calculations and its electronic structure is determined by quantum chemical method for different metal-substituted cluster models. Our calculations showed that the net electron density on the MO_4 unit, where M is Ti^{4+}, Al^{3+}, Ga^{3+}, or Fe^{3+}, is a reliable description of the acidity of metallosilicates. Furthermore, the analysis of MEP values of the cluster models revealed that for prediction of the reactivity of metallosilicates, the MEP map can serve as a sensitive indicator.

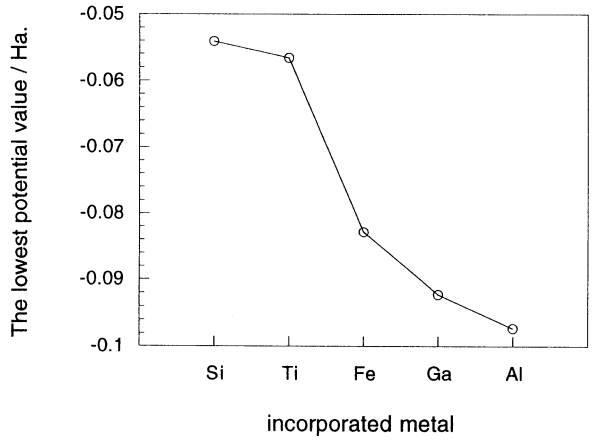

Figure 6. The variation of the minima values in various dimer clusters with different metal atoms in the framework.

References

[1] H. Heinemann, Catal. Rev. Sci. Eng. 23 (1981) 651.
[2] M.E. Davis, C. Saldarriaga, C. Montes, J. Garces and C. Crowder, Nature 331 (1988) 698.
[3] M.E. Leonowicz, J.A. Lawton, S.L. Lawton and M.K. Rubin, Science 264 (1994) 1910.
[4] P. Ratnasamy and R. Kumar, Catal. Today 9 (1991) 329.
[5] A.V. Ramaswamy and S. Sivasanker, Catal. Lett. 22 (1993) 239.
[6] P. Behrens, J. Felsche, S. Vetter, G. Schulz-Ekloff, N.I. Jaeger and W. Niemann, J. Chem. Soc. Chem. Commun. (1991) 678.
[7] D. Trong On, A. Bittar, S. Kaliaguine and L. Bonneviot, Catal. Lett. 16 (1992) 85.
[8] K. Kawamura, in: *Molecular Dynamics Simulations*, eds. F. Yonezawa (Springer, Berlin, 1990) p. 88.
[9] L. Verlet, Phys. Rev. 98 (1967) 159.
[10] P. Ewald, Ann. Phys. 64 (1921) 253.
[11] A. Miyamoto and M. Kubo, Sekiyu Gakkaishi 36 (1993) 282.
[12] A. Miyamoto, H. Himei, Y. Oka, E. Maruya, M. Katagiri, R. Vetrivel and M. Kubo, Catal. Today 22 (1994) 87.
[13] A. Miyamoto, M. Kubo, K. Matsuba and T. Inui, in: *Computer Aided Innovation of New Materials II*, eds. M. Doyama, J. Kihara, M. Tanaka and R. Yamamoto (Elsevier, Amsterdam, 1993) p. 1025.
[14] P. Hohenberg and W. Kohn, Phys. Rev. B 136 (1964) 864.
[15] W. Kohn and L.J. Sham, Phys. Rev. A 140 (1965) 508.
[16] DMol version 2.3.5 (Biosym Technologies, San Diego, 1993).
[17] B. Delley, J. Chem. Phys. 92 (1990) 508.
[18] L. Hedin and B.I. Lundqvist, J. Phys. C 4 (1971) 2064.
[19] A. Becke, J. Chem. Phys. 88 (1988) 2547.
[20] C. Lee, W. Yang and R.G. Parr, Phys. Rev. B 37 (1988) 786.
[21] R. Miura, H. Yamano, R.M. Katagiri, M. Kubo, R. Vetrivel and A. Miyamoto, Catal. Today 23 (1995) 409.
[22] E.G. Derouane and J.J. Fripiat, Zeolites 5 (1985) 165.
[23] A.E. Alvarado-Swaisgood, M.K. Barr, P.J. Hay and A. Redondo, J. Phys. Chem. 95 (1991) 10031.
[24] D.H. Olson, G.T. Kokotailo and S.L. Lawton, J. Phys. Chem. 85 (1981) 2238.
[25] J. Sauer, J. Phys. Chem. 91 (1987) 2315.
[26] H.V. Brand, L.A. Curtiss and L.E. Iton, J. Phys. Chem. 96 (1992) 7725.
[27] A. Chatterjee and R. Vetrivel, Microporous Mater. 3 (1994) 211.
[28] Y. Oumi, K. Matsuba, M. Kubo, T. Inui and A. Miyamoto, Microporous Mater. 4 (1995) 53.
[29] *Kagaku Binran Kisohen II*, eds. Chem. Soc. of Japan (Maruzen, Tokyo, 1993) p. 717.
[30] T. Inui and K. Matsuba, Stud. Surf. Sci. Catal. 90 (1994) 355.
[31] E. Scrocco and J. Tomasi, Adv. Quantum Chem. 11 (1978) 115.
[32] J. Tomasi, in: *Chemical Applications of Atomic and Molecular Electrostatic Potentials*, eds. P. Politzer and D.G. Truhlar (Plenum Press, New York, 1981) p. 151.
[33] G. Náray-Szabó and G.G. Ferenczy, Chem. Rev. 95 (1995) 829.